



Contents lists available at ScienceDirect

## Computational Materials Science

journal homepage: [www.elsevier.com/locate/commatsci](http://www.elsevier.com/locate/commatsci)

# Relationship between thermal conductivity and framework architecture in MOF-5

Luping Han, Makenzie Budge, P. Alex Greaney\*

School of Mechanical, Industrial &amp; Manufacturing Engineering, Oregon State University, Corvallis, OR 97331, United States

## ARTICLE INFO

## Article history:

Received 27 December 2013

Received in revised form 2 June 2014

Accepted 2 June 2014

Available online xxxxx

## Keywords:

Metal–organic-frameworks

Thermal conductivity

Molecular dynamics

## ABSTRACT

Metal–organic-framework materials (MOFs) are the most porous materials known to humanity and thus are promising materials for gas storage and absorption refrigerators—reducing the overall size of the absorption bed. Central to the performance of the MOF is its ability to withdraw heat from the absorbed working gas. Here we use a suite of molecular dynamics simulations to relate structural features of the MOF-5 framework to its thermal transport properties. These were performed for the purpose of establishing design principles that can be used in the development of new MOFs with tailored thermal conductivity. The last part of the paper examines thermal transport in MOF-5 when loaded with hydrogen and deuterium which increases thermal conductivity.

© 2014 Elsevier B.V. All rights reserved.

## 1. Introduction

Metal–organic frameworks (MOFs) are the most porous materials known to humanity, comprised of organic linker molecules assembled into an open network structure through metal–organic connections to nodal junctions [1]. Although metal–organic frameworks are currently attracting intense scrutiny for their exciting potential for gas storage and gas separation, their thermal properties have received limited attention. However, the thermal transport properties of MOFs are both unusual and important, and thus warrant detailed research. Since gas storage and separation processes involve exothermic and endothermic operations [2] the ability to transport heat into or out of the adsorption media can be the limiting factor in the performance of MOFs used in these applications. One beneficial application of MOFs is as the adsorption bed in adsorption chillers [3]. These are cooling systems that are driven by a heat source and use a cycle of evaporation and condensation to pump heat. The use of MOFs as the adsorption bed provides a huge reduction in size that makes chillers practicable for vehicular use when they can be powered by waste engine heat. The motivation for our research on heat transport is a second important application of MOFs—hydrogen storage in MOF-5.

Hydrogen storage devices using powder compacts of MOF-5 crystals as the adsorption bed are under development as part of the US Department of Energy's (DoE) Hydrogen Fuel Cell Program.

These tanks are liquid nitrogen cooled and pressurized to 100 bar, and under these conditions can store 7% excess wt% of H which amounts to 215 H<sub>2</sub> dimers per unit cell of the MOF, or an average of 26.9 dimers per framework cage [2]. This yields comparable storage density to liquefied H<sub>2</sub>, but at a more practicable temperature. The limitations for these devices is not capacity but the refueling time. MOF-5 has poor thermal conductivity (0.31 W/m K [4], similar to concrete) and this impedes the removal of latent heat of adsorption [2,5]. Currently, to meet DoE's performance targets for H<sub>2</sub> storage, at least a fivefold increase in thermal conductivity is required [6,7].

Heat transport in MOF-5 is unusual. Heat is carried by both transfer between localized molecular modes (like in an amorphous polymer) and by propagating lattice-modes (like in a crystalline solid). Kaviany and co-workers have performed an excellent computational study of thermal transport in MOF-5, characterizing the transport mechanisms and determining that the molecular-mode and lattice-mode heat currents contribute roughly equally to the thermal conductivity [8].

In this research, our goal is to establish design principles that will guide the development of new gas storage MOFs with improved thermal conductivity. Thus, we extend the work of Kaviany et al. to examine strategies for changing the MOF architecture. To design MOFs that mitigate the thermal transport bottleneck it is imperative to understand the relationship between the structure of the framework and *both* of the heat transport mechanisms. In this manuscript we report the results of a systematic molecular dynamics study on the sensitivity of thermal conductivity to variations in the MOF architecture. We also present a new approach to

\* Corresponding author. Tel.: +1 541 737 3048.

E-mail address: [alex.greaney@oregonstate.edu](mailto:alex.greaney@oregonstate.edu) (P. Alex Greaney).URL: <http://research.engr.oregonstate.edu/greaney/>

obtaining mechanistic information by spatially decomposing the heat current. The remainder of the article is organized as follows: After a brief description of the simulation methods and philosophy, we present and discuss the simulation results for empty MOFs. We then discuss simulations of MOF-5 filled with  $H_2$ . The article finishes with a summary and conclusions.

## 2. Method

Thermal conductivity,  $\kappa$ , of MOFs was computed from equilibrium classical molecular dynamics (MD) simulations in the micro-canonical ensemble using the Green–Kubo method [9,10]. This is a well established method based on the fluctuation dissipation theorem that relates the thermal conductivity to the integral of the autocorrelation function (ACF) of the instantaneous heat flux.

$$\kappa = \frac{V}{3k_B T^2} \int_0^\infty dt \langle \mathbf{J}(t) \cdot \mathbf{J}(t + \tau) \rangle, \quad (1)$$

This can be likened to “measuring” the thermal conductivity from a computer simulation, rather than a mechanism based prediction of  $\kappa$  as one obtains using Boltzmann transport theory. Our approach is to use simulations as a computer experiment, in which we vary various aspects of the MOFs and determine the impact on  $\kappa$ . In these experiments we decompose the heat current  $\mathbf{J}$  into different local contributions,

$$\mathbf{J} = \sum_i \mathbf{J}_i \quad (2)$$

where  $\mathbf{J}_i$  is the instantaneous heat current in region  $i$ . The contributions of the regional autocorrelations and the inter-regional cross-correlation to  $\kappa$ ,

$$\langle \mathbf{J}(t) \cdot \mathbf{J}(t + \tau) \rangle = \sum_{ij} \langle \mathbf{J}_i(t) \cdot \mathbf{J}_j(t + \tau) \rangle, \quad (3)$$

are used to infer mechanistic changes to the heat transport processes. We have recently successfully used a similar spatial decomposition of  $\mathbf{J}$  to map heat transport around defects in graphite [11].

All simulations are performed on a  $2 \times 2 \times 2$  super cells with periodic boundary conditions. (A single unit cell of the frameworks and their components is shown in Fig. 1.) For the empty MOF-5 calculations this is a cubic compute cell with  $\sim 52$  Å edges containing 3392 atoms. The previous work by Kaviani et al. has shown that a  $2 \times 2 \times 2$  super cell is sufficiently large to obtain converged predictions for  $\kappa$ , and in this research we have independently corroborated this. For their study of MOF-5, Kaviani et al. developed a set of empirical interatomic potentials for modeling the Zn, O, and C atoms in the framework (H they included indirectly by increasing the mass of the carbon with attached H atoms). We have tested these potentials against the Hessian matrix for MOF-5 computed from first principles. (The Hessian was computed using the SIESTA density functional theory package [12] with a DZP or better basis using the PBE generalized gradient exchange correlation energy functional [13]. Calculations were performed with a 700 Rydberg energy cutoff and the structure relaxed to minimize forces to a tolerance of 0.01 eV/Å<sup>2</sup>.)

To correctly simulate the MOF interacting with gases intercalated into the framework we must model the H in the framework explicitly. Thus, we have augmented Kaviani’s potentials with a set of bonding, angular, and dihedral terms for the H. These are listed in Table 1. Additionally, Kaviani’s potential set does not include a C–C–O angular interaction at the end of the linkers. This means the framework has no resistance to in-plane bending of the linkers at the node-linker bridge, making the framework overly soft in shear along the (110) directions. We have included a C–C–O angular term. For most of the simulations we have kept this

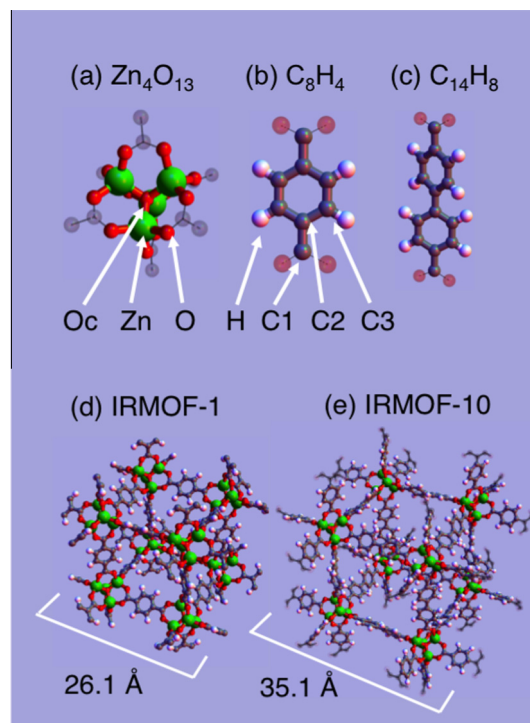


**Fig. 1.** (a–c) Shows the components of the IRMOF-1 (also called MOF-5) and IRMOF-10 frameworks. (a) Shows the  $Zn_4O_{13}$  nodal units, (b) the  $C_8H_4$  (1,4 phenyl dicarboxylate) linkers in IRMOF-1, and (c) the  $C_{14}H_8$  (4,4 biphenyl dicarboxylate) linkers in IRMOF-10. (d and e) Show a single unit cell of each framework. Note that along each direction the orientation of the nodes alternates and so there are 8 nodes per unit cell. This alternating structure means there are two types of interstitial cage.

turned off in order to compare our work with that of Kaviani et al. However, we have also computed  $\kappa$  with the extra angular stiffness turned on—the results are described in the next section. The non-bonded potentials for H were those used in the code AutoDock and the added bonding terms were chosen to match the full Hessian matrix of MOF-5 that was computed from first principles.

All simulations were performed at 300 K. The simulation procedure was as follows: The empty MOF structure was optimized at 0 K. The  $2 \times 2 \times 2$  supercell was created and simulated in the NPT ensemble under zero pressure with the cell free to change volume but not shape. The temperature was ramped slowly to 400 K. From this simulation a fit was performed to obtain the thermal expansion coefficient for the potentials used (which is negative [14,15]). For each simulation the  $2 \times 2 \times 2$  super cell was scaled to its mean volume at 300 K and then heated to 300 K in the NVT ensemble, before being allowed to equilibrate by simulation for 100 ps in the NVE ensemble. After equilibration, NVE simulation was continued for a further 500 ps during which the heat flux was computed and its autocorrelation function averaged. The autocorrelation was computed out to 10 ps or longer, and at least 40 simulations with different starting configurations were averaged to obtain each datum.

In simulations with gas atoms in the framework, the gas molecules were placed randomly in the framework interstices with random orientation (any randomly chosen positions that would have placed atoms too close together were rejected). The gas loaded framework was optimized and annealed prior to the NVT heating step to 300 K described above. Note that when we added the gas we did not alter the volume of the framework. At 300 K the gas condenses onto the framework and is not mobile across the voids within the framework. As a result, the gas put the framework

**Table 1**

Augmented interatomic potentials used to simulate MOF-5 and IRMOF-10. The cutoff of non-bonded interactions is 10 Å.

Type	Potential	Parameters
<i>Atom labels</i>		
H2	Hydrogen (or deuterium) in H <sub>2</sub> (D <sub>2</sub> ) dimer guest molecules	
Oc	O in node center	
Zn	Zinc in node	
O	Node-linker bridging oxygen	
C1	Terminal carbon	
C2	C–C <sub>3</sub> in phenyl	
C3	C–C <sub>2</sub> H in phenyl	
H	Hydrogen in phenyl ring	
<i>Bonds</i>		
H2–H2	$E = K(r - r_0)^2$	$K = 1.85 \text{ eV } \text{Å}^{-2}, r_0 = 0.74 \text{ Å}$
C3–H	$E = K(r - r_0)^2$	$K = 17.04 \text{ eV } \text{Å}^{-2}, r_0 = 1.10 \text{ Å}$
<i>Angles</i>		
C2/3–C3–H	$E = K(\theta - \theta_0)^2$	$K = 1.6 \text{ eV}, \theta_0 = 120^\circ$
O–C1–C2	$E = K(\theta - \theta_0)^2$	$K = 3.0 \text{ eV}, \theta_0 = 120^\circ$ (when turned on)
<i>Dihedrals</i>		
C3–C2–C2–C3	$E = K[1 + d \cos(n\phi)]$	$K = 0.434 \text{ eV}, d = -1, n = 2$
C2–C2–C3–H	$E = K[1 + d \cos(n\phi)]$	$K = 0.130 \text{ eV}, d = -1, n = 1$
C2–C2–C3–C3	$E = K[1 + d \cos(n\phi)]$	$K = 1.735 \text{ eV}, d = 1, n = 1$
<i>Non-bonded interactions</i>		
H2–H2	$E = 4\epsilon \left( \left( \frac{r}{r_0} \right)^{12} - \left( \frac{r}{r_0} \right)^6 \right)$	$\epsilon = 0.00087 \text{ eV}, r_0 = 2 \text{ Å}$
H2–Oc	$E = 4\epsilon \left( \left( \frac{r}{r_0} \right)^{12} - \left( \frac{r}{r_0} \right)^6 \right)$	$\epsilon = 0.00750 \text{ eV}, r_0 = 3.6 \text{ Å}$
H2–Zn	$E = 4\epsilon \left( \left( \frac{r}{r_0} \right)^{12} - \left( \frac{r}{r_0} \right)^6 \right)$	$\epsilon = 0 \text{ eV}, r_0 = 0 \text{ Å}$
H2–O	$E = 4\epsilon \left( \left( \frac{r}{r_0} \right)^{12} - \left( \frac{r}{r_0} \right)^6 \right)$	$\epsilon = 0.00750 \text{ eV}, r_0 = 3.6 \text{ Å}$
H2–C1	$E = 4\epsilon \left( \left( \frac{r}{r_0} \right)^{12} - \left( \frac{r}{r_0} \right)^6 \right)$	$\epsilon = 0.01089 \text{ eV}, r_0 = 4.0 \text{ Å}$
H2–C2	$E = 4\epsilon \left( \left( \frac{r}{r_0} \right)^{12} - \left( \frac{r}{r_0} \right)^6 \right)$	$\epsilon = 0.01089 \text{ eV}, r_0 = 4.0 \text{ Å}$
H2–C3	$E = 4\epsilon \left( \left( \frac{r}{r_0} \right)^{12} - \left( \frac{r}{r_0} \right)^6 \right)$	$\epsilon = 0.01089 \text{ eV}, r_0 = 4.0 \text{ Å}$
H2–H	$E = 4\epsilon \left( \left( \frac{r}{r_0} \right)^{12} - \left( \frac{r}{r_0} \right)^6 \right)$	$\epsilon = 0.00390 \text{ eV}, r_0 = 3.0 \text{ Å}$

under small *tensile* pressure as the gas acts to slightly contract the framework. Simulations were performed using the LAMMPS molecular dynamics simulation package [16]. Trajectories were integrated using the velocity verlet method with a time step of 0.2 fs, which was sufficient to minimize total energy fluctuations during NVE simulation to less than  $10^{-5}$  of the thermal energy.

### 3. Dependence of $\kappa$ on framework architecture

To establish a set of design principles that can be used in the development of new gas storage MOFs with improved thermal transport properties we must understand how aspects of the framework structure impact heat transport by both molecular modes and by lattice modes. We consider four separate factors: The acoustic mismatch between the nodes and linker arms; the stiffness of the framework in shear; the effect of putting the system in tension; and the effect of the linker arm length.

#### 3.1. Node-linker acoustic mismatch

Heat transport by molecular modes is passed between localized molecular vibrations. To move through the MOF the heat must be passed from modes in the linkers to modes in the nodes. The node is much heavier than the linker. The nodes and linkers are acoustically mismatched creating a bottleneck for the molecular-mode heat transport. We have tuned the acoustic mismatch by scaling the mass of atoms in either the nodes (Zn, O and Oc) or the linkers (C1, C2, C3 and H). The thermal conductivity with mass scaling is

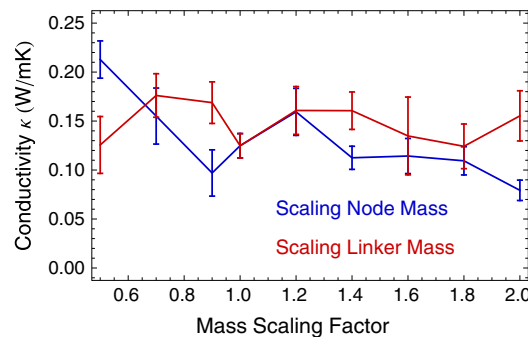


**Fig. 2.** Thermal conductivity of MOF-5 as a function of scaling the mass of selected components of the lattice. The blue plot shows scaling the mass of nodes (atoms Oc, Zn, and O). The red plot shows scaling the mass of the linker atoms (C1, C2, C3, and H). (For interpretation of the references to colour in this figure legend, the reader is referred to the web version of this article.)

shown in Fig. 2. Sweeping the mass of the nodal atoms through a fourfold scaling from half to twice their normal mass increases the acoustic mismatch between the linkers and nodes and produces nearly a twofold reduction in thermal conductivity (discernable even though the error bars are large). Reducing the mass of the node atoms reduces the frequency of the nodes' internal molecular modes, and so reduces the acoustic mismatch with the linker. Increasing the mass of the linker atoms should also reduce the acoustic mismatch; however, as is shown in Fig. 2 this results in very little change in  $\kappa$  discernable above the noise in the error bars.

It is clear from the mass scaling calculations that node-linker acoustic mismatch is only one factor affecting heat transport. We have computed the eigenvalues of the mass weighted Hessian matrix as a function of scaling the node or linker masses. It was found that as the nodes are much heavier than the linkers the mass of the node atoms have a strong influence on the lattice mode dispersion. Increasing the node mass affects both the molecular-mode and lattice mode heat current adversely. Increasing the linker mass improves molecular mode thermal conductivity but degrades the lattice mode thermal conductivity, and although  $\kappa$  changes little the spectral make up of the heat current ACF is different as can be seen in Fig. 3. It can be seen in Fig. 3(c) that changing the mass of the node or linker atoms has a large impact on the high frequency component of the heat current, however the high frequency fluctuations carry little heat.

The relative importance of lattice and molecular modes is determined by fitting an approximate form of the ACF,  $C_f$ , in fourier space with the sum of decaying oscillatory processes:

$$C_f(t) = \sum_i A_i \cos(2\pi\nu_i t) e^{-t/\tau_i},$$

with amplitudes  $A$ , frequencies  $\nu$ , and decay times  $\tau$  as fitting parameters. In this approximation each process contributes

$$\kappa_i = \frac{V}{3k_B T^2} \frac{A_i \tau_i}{1 + (2\pi\nu_i \tau_i)^2}$$

to the total thermal conductivity. As heat current fluctuation processes are all underdamped, increasing the lifetime—that is, sharpening the peak in the power spectrum—reduces the contribution to thermal conductivity.

#### 3.2. Framework shear stiffness

Simulations were performed to measure  $\kappa$  of MOF-5 with and without the angular O–C1–C2 interaction at the node-linker bridge. The angular interaction stiffens the shear modulus of the framework, but surprisingly does little to change  $\kappa$ . While net  $\kappa$

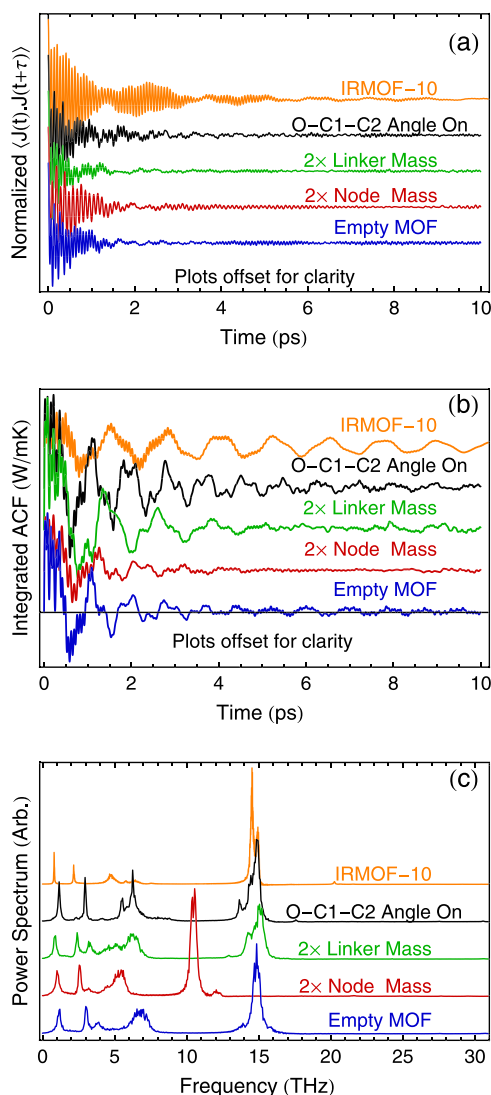


**Fig. 3.** Plot (a) shows the averaged heat flux ACF for different MOFs. Plot (b) shows the integration of the ACF as a function of the integration duration. Plot (c) shows the power spectrum of heat current. In all plots (a–c) the curves are normalized and offset for clarity. The blue, red, green, black and orange traces are for: empty MOF-5, MOF-5 with heavy nodes; MOF-5 with heavy linkers; MOF-5 with the O–C1–C2 angular interaction turned on; and for IRMOF-10. (For interpretation of the references to colour in this figure legend, the reader is referred to the web version of this article.)

is altered, the angular interaction changes the nature of the thermal fluctuations—resulting in different spectral make-up and slower convergence of the heat current ACF shown in Fig. 3(a–c). The angular interaction also makes a small, but statistically significant, change to the cross-correlation of the linker and node heat flux. As can be seen in Fig. 5, turning on this extra angular stiffness makes the node-linker cross-correlation have a positive rather than negative impact on the thermal conductivity.

### 3.3. Effect of strain on $\kappa$

We have measured (*in silico*) the effect of homogeneous strain on the thermal transport. Strains can arise from many sources; MOF-5 thermally contracts, and gas storage applications put MOFs under pressure—the working pressure for the MOF-5 based  $H_2$  storage device is 100 bar. Moreover, we have found that MOF-5 contracts with the uptake of gas. The gas molecules bind to the

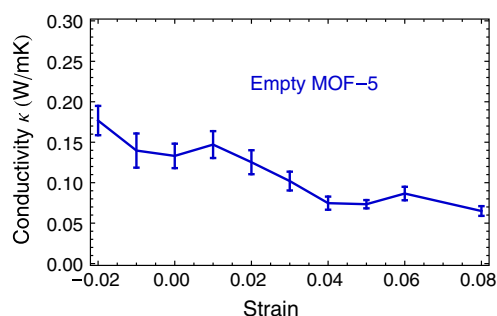


**Fig. 4.**  $\kappa$  of MOF-5 computed as a function of strain.

framework preferentially at the “oxter”<sup>1</sup> where the linkers come together at a node and the gas molecules can interact with several linkers simultaneously. This interaction pinches the junctions causing contraction of the framework. Thermal contraction is due to activation of soft buckling modes in the linker arms [14,15], and thus one might anticipate that—like tuning a guitar string—putting the linkers in tension would increase the lattice-mode thermal conductivity. In this reasoning the effect of strain would be asymmetric due to linker buckling under compression. Surprisingly, we observe only small systematic change in  $\kappa$  due to strain with tension reducing the ease of heat transport, as shown in Fig. 4.

### 3.4. Expanding linker arm length

The topology of the framework proscribes that heat transported by molecular-modes must flow through the thermally resistive bridge between nodes and linkers. We exploit this to probe the interplay of molecular-mode and lattice-mode heat transport. If the resistance to molecular-mode heat transport is dominated by linker-node acoustic mismatch, then extending the length of linkers will increase the molecular-mode conductivity along a chain of links by reducing the number of resistive interfaces along each linker direction. However, increasing the linker length also reduces the areal density of linkers cutting through any cross-section of the framework. The density of heat conducting channels goes down faster than their thermal conductivity rises, and so one obtains a net reduction in the molecular mode thermal conductivity  $\kappa_M$  that scales with the framework’s lattice parameter,  $a$ , as  $\kappa_M \sim a^{-1}$ . The beautiful modular chemistry of MOFs permits us to change  $a$  by inserting longer linker arms while maintaining the topology, symmetry, and nodal chemistry. We have simulated IRMOF-10 (isoreticular-MOF) in which phenyl groups are substituted with biphenyl [17]. (MOF-5 is the first in IRMOF series and is also called IRMOF-1 [18].) Simulating IRMOF-10 requires three new dihedral terms which are included in Table 1.

The heat flux ACF and the resulting thermal conductivity value for IRMOF-10 are shown in Figs. 2 and 5. The heat current ACF and its integral contains long slow oscillations that are slow to die out. To obtain converged results it was necessary to compute the ACF for IRMOF-10 out to 50 ps. The thermal conductivity of IRMOF-10 was less than one quarter of that of MOF-5. The lattice parameter of MOF-5 is only 0.75 times smaller than that of IRMOF-10, and so the reduction in  $\kappa$  cannot be explained by the density of node-linker thermal bottlenecks alone (although it is possible that the phenyl-to-phenyl link at the center of the biphenyl linkers also introduces a thermal bottleneck for molecular modes). The longer lived fluctuations have a slower decay rate (as indicated by the sharper peaks in Fig. 3(c)), and as these are in the under damped limit increasing the fluctuation lifetime reduces the contribution to heat transport (Eq. (1)).

<sup>1</sup> An old Scottish word for armpit.

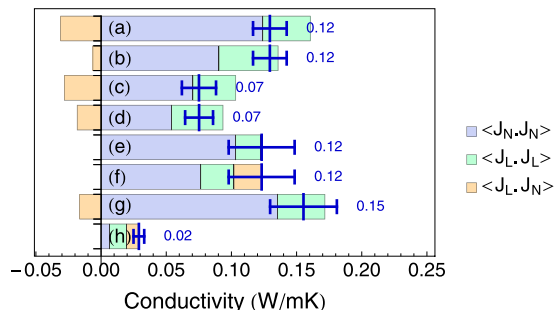


**Fig. 5.** Bar chart of the thermal conductivity of frameworks, including the contributions from the autocorrelation of the heat current in nodes and linkers, and the node-linker heat current cross-correlation. (a and b) Are for empty MOF-5, (c and d) are for MOF-5 with the mass of the Oc, Zn and O atoms doubled, and (e and f) are for MOF-5 with the O–C1–C2 angular interaction turned on. In (a, c, and, e) the O atoms are included in the calculation of  $J_N$ , and in (b, d, and f) it is included in  $J_L$ . Plot (g) is for MOF-5 with the mass of C1, C2, C3, and H doubled (and O included in  $J_N$ ). Plot (h) is for IRMOF-10 with O included in  $J_L$ . The dark blue line indicates the total thermal conductivity for the framework with error bars. (For interpretation of the references to colour in this figure legend, the reader is referred to the web version of this article.)

### 3.5. Decomposition of $J$

We analyse equilibrium MD simulations by decomposing the heat current,  $J = J_N + J_L$ , into contributions from the nodes,  $J_N$ , and contributions from the linkers,  $J_L$ , and integrating the correlation functions (see Fig. 5). A number of interesting observations arise from the contribution of these integrated correlation functions to  $\kappa$ .

- Increasing the mass of node atoms reduces the contribution of  $\langle J_N \cdot J_N \rangle$  to  $\kappa$ .
- The cross-correlation in Fig. 5(a–d, and g) is negative. This implies that there is considerable reflection of heat current fluctuations at the interface between nodes and linkers.
- For MOF-5 the cross-correlation is most negative when O is considered part of the linker. This indicates that most of the reflection occurs at the interface between O and Zn. This interface also has the largest mass difference.
- Increasing the linker length from MOF-5 to IRMOF-10 greatly reduces  $\kappa$  and changes the relative contributions of  $\langle J_N \cdot J_N \rangle$ ,  $\langle J_L \cdot J_L \rangle$ , and  $\langle J_N \cdot J_L \rangle$ .
- Turning on the O–C1–C2 angular interaction does not change  $\kappa$  (at least within the resolution of the error bars), however Fig. 5(b and d) show a statistically significant change in the contribution from the cross-correlation  $\langle J_N \cdot J_L \rangle$ . This result illustrates an important difficulty for validation of computational prediction of thermal conductivity—namely that  $\kappa$  is an integral property and so it is possible to obtain the correct answer for the wrong reasons. Simply predicting a value of  $\kappa$  that matches experiment is insufficient to demonstrate the validity of the model that made the prediction.

### 4. Gas filled framework

MOFs used for gas storage will, by definition, be filled with gas. As it is the removal of latent heat of adsorption that limits gas uptake, it is important to determine the role that framework guests play in thermal transport. Simulations were performed of MOF-5 at 300 K, loaded with hydrogen and deuterium, up to an average 14 dimers per framework cage. Under these conditions the gas is bound to the framework and while the dimers migrate along the linker arms, there is little free motion across the voids of the framework. A typical simulation system is shown in Fig. 6 along with the plot of  $\kappa$  as a function of gas concentration. Adding  $H_2$

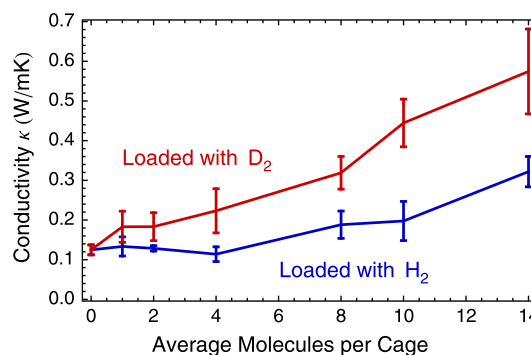
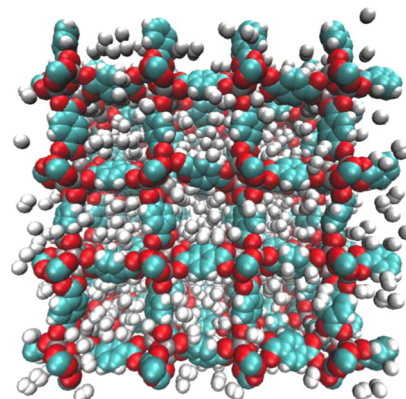


**Fig. 6.** (Top) Example of the  $2 \times 2 \times 2$  supercell structure of MOF-5 loaded with  $H_2$  molecules (image is prior to annealing). (Bottom) Plot of thermal conductivity of MOF-5 as a function of loading with hydrogen and deuterium.

causes a modest increase in  $\kappa$ , along with a small tensile stress. The surprising negative response to strain in Fig. 4 indicates that this increase in  $\kappa$  is not due to stress. Furthermore, we have computed  $J_G$ , the heat current involving gas atoms, and find correlations involving  $J_G$  make a negligible contribution to  $\kappa$ .

Adding deuterium to the system instead of  $H_2$  gives a larger increase in  $\kappa$ , showing that the mass of the gas is important. Gas in the framework adds disorder to the system increasing scattering of lattice modes. However, as the gas binds preferentially to the outer of the linkers, we attribute the increase in  $\kappa$  to the gas providing additional channels for heat transfer from nodes to linkers.

### 5. Conclusions and summary

In this paper we have presented a systematic study of the interplay of MOF architecture with heat transport mechanisms. It was found that many aspects of the framework impact both the molecular-mode and lattice-mode transport processes. Specifically, changing the linker mass and increasing the shear stiffness through the O–C1–C2 angular interaction produce little change in  $\kappa$ . In both of these cases simulations show very different dynamics in the heat current fluctuations. We thus conclude that changes to  $\kappa$  are buffered, because the linker mass and the O–C1–C2 angle affect the lattice and molecular modes in opposite directions. To engineer a substantial net change in  $\kappa$  it is necessary to identify parameters that change both heat transport mechanisms in the same direction. In this work we have found two such parameters: the node mass, and the linker arm length. The lattice-mode and molecular-mode thermal conductivity are both reduced by increasing the mass of nodes and the lengthening linker arms.

We have presented a new approach to analyzing equilibrium molecular dynamics simulations to obtain insight into heat transport mechanisms. This approach is based on the Green–Kubo

method and involves spatially decomposing the instantaneous heat current, and computing the regional autocorrelations and cross-correlations separately. The sign of the cross-correlation reveals information about heat transfer between regions.

Finally, it was found that the thermal conductivity is increased by loading MOF-5 with gas, with  $\kappa$  increasing with both the concentration and mass of the adsorbed gas. This result is beneficial for many gas adsorption applications where the rate of adsorption is limited by the removal of latent heat. A more complete understanding of the mechanisms of adsorbate-enhanced thermal transport will facilitate design of MOFs with desired thermal properties, and so this is an area of continued research.

### Acknowledgments

This work used the Extreme Science and Engineering Discovery Environment (XSEDE), which is supported by National Science Foundation Grant No. OCI-1053575.

### References

- [1] O.M. Yaghi, M. O'Keeffe, N.W. Ockwig, H.K. Chae, M. Eddaoudi, J. Kim, *Nature* 423 (2003) 705–714.
- [2] J. Zhang, T.S. Fisher, P.V. Ramachandran, J.P. Gore, I. Mudawar, *J. Heat Transfer* 127 (12) (2005) 1391.
- [3] X. Sun, C.D. Wick, P.K. Thallapally, B.P. McGrail, L.X. Dang, *J. Phys. Chem. B* 115 (12) (2011) 2842–2849.
- [4] B. Huang, Z. Ni, A. Millward, A. McGaughey, C. Uher, M. Kaviani, O. Yaghi, *Int. J. Heat Mass Transfer* 50 (2007) 405–411.
- [5] J. Purewal, D. Liu, A. Sudik, M. Veenstra, J. Yang, S. Maurer, U. Müller, D.J. Siegel, *J. Phys. Chem. C* 116 (2012) 20199–20212.
- [6] G.O. Carole Read, George Thomas, D.S. Satyapal, *Mater. Matters* 2 (2007) 3.
- [7] Fuel cell technologies office multi-year research, development and demonstration plan. Section 3.3 Hydrogen Storage, 2012.
- [8] B. Huang, A. McGaughey, M. Kaviani, *Int. J. Heat Mass Transfer* 50 (3–4) (2007) 393–404.
- [9] M.S. Green, *J. Chem. Phys.* 22 (1954) 398–413.
- [10] R. Kubo, *J. Phys. Soc. Jpn.* 12 (6) (1957) 570–586.
- [11] Mapping thermal resistance around vacancy defects in graphite, vol. 1543, 2013.
- [12] J.M. Soler, E. Artacho, J.D. Gale, A. García, J. Junquera, P. Ordejón, D. Sánchez-Portal, *J. Phys.: Condens. Matter* 14 (11) (2002) 2745.
- [13] J.P. Perdew, K. Burke, M. Ernzerhof, *Phys. Rev. Lett.* 77 (1996) 3865–3868.
- [14] N. Lock, Y. Wu, M. Christensen, L.J. Cameron, V.K. Peterson, A.J. Bridgeman, C.J. Kepert, B.B. Iversen, *J. Phys. Chem. C* 114 (2010) 16181–16186.
- [15] N. Lock, M. Christensen, Y. Wu, V.K. Peterson, M.K. Thomsen, R.O. Piltz, A.J. Ramirez-Cuesta, G.J. McIntyre, K. Noren, R. Kutteh, C.J. Kepert, G.J. Kearley, B.B. Iversen, *Dalton Trans.* 42 (2013) 1996–2007.
- [16] S. Plimpton, *J. Comput. Phys.* 117 (1995) 1–19. <<http://lammps.sandia.gov>>.
- [17] M. Eddaoudi, J. Kim, N. Rosi, D. Vodak, J. Wachter, M. O'Keeffe, O.M. Yaghi, *Science* 295 (5554) (2002) 469–472.
- [18] M. Eddaoudi, D.B. Moler, H. Li, B. Chen, T.M. Reineke, M. O'Keeffe, O.M. Yaghi, *Acc. Chem. Res.* 34 (4) (2001) 319–330. PMID: 11308306.